Observation of a Spontaneous Particle-Transport Barrier in the HL-2A Tokamak

W. W. Xiao (肖维文),[1] X. L. Zou (邹晓岚),[2] X. T. Ding (丁玄同),[1] L. H. Yao (姚良骅),[1] B. B. Feng (冯北滨),[1] X. M. Song (宋显明),[1] S. D. Song (宋绍栋),[2] Y. Zhou (周艳),[1] Z. T. Liu (刘泽田),[1] B. S. Yuan (袁宝山),[1] H. J. Sun (孙红娟),[1] X. Q. Ji (季小全),[1] Y. D. Gao (高亚东),[1] Y. G. Li (李永高),[1] L. W. Yan (严龙文),[1] Q. W. Yang (杨青巍),[1] Yi Liu (刘仪),[1] J. Q. Dong (董家齐),[1] X. R. Duan (段旭如),[1] Yong Liu (刘永),[1] C. H. Pan (潘传红),[1] and HL-2A Team

[1]*Southwestern Institute of Physics, P.O. Box 432, Chengdu, China*

[2]*CEA, IRFM, F-13108 Saint-Paul-lez-Durance, France*

(Received 5 June 2008; published 24 May 2010)

Using the profile analysis, the density perturbation transport analysis, and the Doppler reflectometry measurement, for the first time a spontaneous and steady-state particle-transport barrier has been evidenced in the Ohmic plasmas in the HL-2A tokamak with no externally applied momentum or particle input except the gas puffing. A threshold in density has been found for the observation of the barrier. The particle diffusivity is well-like, and the convection is found to be inward outside the well and outward inside the well. The formation of the barrier coincides with the transition between the trapped electron mode and the ion temperature gradient driven mode.

DOI: 10.1103/PhysRevLett.104.215001 PACS numbers: 52.55.Fa, 52.25.Fi

Intensive effort has been made for experimental as well as theoretical studies of the particle transport in tokamaks, which has a direct impact on subjects such as energy confinement, particle fueling, impurity control, etc. Particle-transport barriers with energy confinement improvement have been observed in tokamaks, such as the H mode [1] at the edge of the plasma and internal transport barrier (ITB) [2–5] in the core. These regimes have often been obtained with high power external input auxiliary heating as the neutral beam injection [1,5], off-axis minority ion-cyclotron heating [3,4], or large external input particle source as the pellets [2]. The mechanisms responsible for these barriers are reversed magnetic shear, or $E \times B$ rotation shear. In this Letter we report the observation of a spontaneously generated particle-transport barrier in purely Ohmically heated plasmas in the HL-2A tokamak with no externally applied momentum or particle input, except the standard gas puffing.

The plasma parameters in the present experiments are major radius $R = 1.64$ m, minor radius $a = 0.40$ m, toroidal magnetic field $B_T = 1.45$ T, and plasma current $I_p = 185$ kA. The plasma is circular with limiter configuration. The density profile is measured by a broadband O mode reflectometer of 26.5–40 GHz, which covers a density domain of 0.8 to 2.0×10^{19} m^{-3}. The line averaged density is measured by a hydrogen cyanide interferometer. The electron temperature is measured by the diagnostic of electron cyclotron emission.

Internal particle-transport barriers (pITBs) have been observed in stationary Ohmic plasmas in the HL-2A tokamak with or without standard gas puffing. This phenomenon is perfectly reproducible. Figure 1 shows a steady state of the pITB over a time of 400 ms, much longer than the energy confinement time ($\tau_E \approx 60$ ms). The parameter characterizing the pITB is the normalized density gradient $-a\nabla n_e/n_e = a/L_n$. Figure 1(a) (in the bottom) displays the time-space evolution of the density gradient, showing clearly the trace of pITB around $r = 0.29$ m for a nearly constant line averaged density $\bar{n}_e = 3.0 \times 10^{19}$ m^{-3}. Figure 1(b) shows the density profile at selected times: before the formation of the barrier ($\bigcirc$ $t_0 = 240$ ms), during the barrier phase with gas puffing ($t_1 = 520$ ms, $t_2 = 670$ ms), and without gas puffing ($t_3 = 790$ ms, $t_4 = 832$ ms). From this figure it can be observed that the pITB remains unchanged even though the gas puffing is stopped. This shows unambiguously that the pITB formation does not depend on the gas puffing.

Figure 2(c) displays the time-space evolution of the density gradient when the density increases slowly. It shows clearly the trace of pITB around $r = 29$ cm. Before $t = 400$ ms, no clear barrier has been observed. Starting from this time, the pITB appears progressively. The critical density corresponding to this transition is $\bar{n}_c = 2.2 \times 10^{19}$ m^{-3}. After the injection of a particle pulse by super-

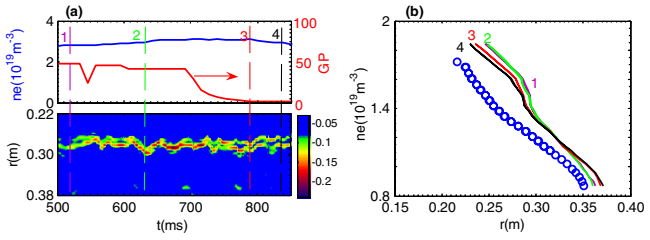

FIG. 1 (color online). Shot no. 7243. (a) Central line averaged density, the gas puffing (GP) signal (in arbitrary units), and the time-space evolution of the density gradient. (b) Density profile at selected times, before the formation of the barrier ($\bigcirc$ $t_0 = 240$ ms), during the barrier phase with gas puffing ($t_1 = 520$ ms, $t_2 = 670$ ms), and without gas puffing ($t_3 = 790$ ms, $t_4 = 832$ ms).

 © 2010 The American Physical Society

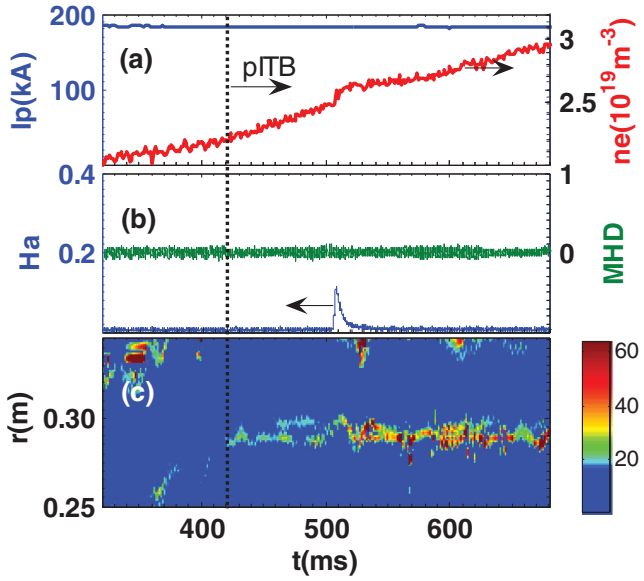

FIG. 2 (color). Shot no. 7557. (a) Plasma current I_p, the central line averaged density. (b) Mirnov coil signal and H_α signal (in arbitrary units). (c) Time-space evolution of the density gradient.

sonic molecular beam injection (SMBI) [6] at $t = 510$ ms, identified by a sharp increase of the H_α signal, the pITB trace is much more visible, and the density gradient is steeper.

Figure 3 shows the density gradient length at $t = 465$ ms. The width of the barrier is 1–2 cm. A drastic change has been observed in the density gradient through this barrier: $L_n \approx 0.1$ m at the barrier location, $L_n \approx 0.5$ m inside the barrier, and $L_n \approx 0.25$ m outside the barrier. In a region without particle sources and in steady state, the particle flux $\Gamma = -D\nabla n_e - Vn_e \approx 0$, where D is the particle diffusivity, V is the particle convective velocity defined as positive for inward (pinch) and negative for outward, and the ratio D/V is directly equal to L_n, $L_n = D/V$. Thus the barrier observed here is well-like and not steplike. Because of the space resolution of the electron cyclotron emission diagnostic, which is about 3 cm, larger than the barrier width (1–2 cm), even though no significant change has been observed in the temperature profile during the pITB formation, we cannot conclude that there is no heat transport barrier accompanying the pITB.

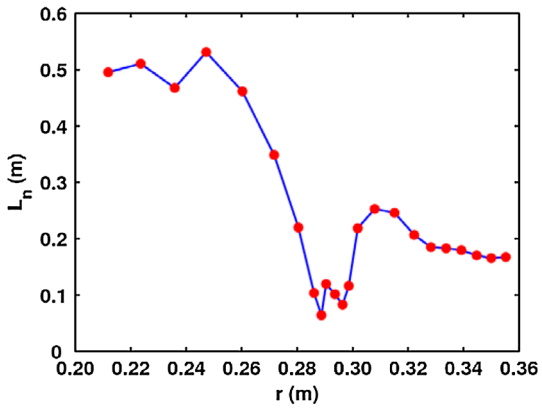

FIG. 3 (color online). Shot no. 7557. Density gradient length at $t = 465$ ms.

A simple profile analysis does not allow us to separate D and V. Modulation of auxiliary heating (electron cyclotron resonance heating, ion cyclotron resonance heating) is a powerful tool for the investigation of the heat transport [7–9] and the heat ITB [10]. Initially the SMBI has been conceived for fueling in tokamaks with better efficiency than the gas puffing. However, in our experiments the SMBI is used as a simple tool for the density modulation. These experiments normally allow us to separate the diffusivity term and the convection term, by using the fact that, on one hand, the phase of the particle wave generated by the modulation is very sensitive to the diffusivity but less sensitive to the convection, and on the other hand, the amplitude of the particle wave is sensitive to diffusivity but very sensitive to the convection [7].

SMBI modulation experiments have been performed for the stationary plasma regime with pITB. In the present case (shot no. 7593), the transport analysis with SMBI modulation has been carried out over a time interval from 400 to 800 ms, in which the time-averaged density is nearly constant, $\bar{n}_e \approx 2.5 \times 10^{19}$ m^{-3}. The SMBI modulation frequency is 9.6 Hz, the duration of SMBI pulse is about 6 ms, and the beam source pressure of SMBI is 1.3 MPa. It should be noted that the pITB phenomenon is not transient, but steady state (much longer than the modulation period). It is also not generated by the SMBI. Furthermore the pITB is robust enough and not destroyed by the SMBI, and thus it can be investigated by it. The amplitude of the density perturbation is about 10%–20%. The time resolution of the reflectometry is 1 ms. Figures 4(a) and 4(b) display, respectively, the phase and the amplitude of the first harmonic of the Fourier transform of the density modulated by SMBI. From Fig. 4(a), the minimum of the phase is at $r \approx 0.253$ m, which generally determines the particle source location. An empirical scaling law of the penetration depth for SMBI has been found in the HL-2A tokamak [11]: $\lambda/a = C\bar{T}_e^{-0.6}$ (keV)$\bar{n}_e^{-0.2}(10^{19}$ m$^{-3})P_0^{0.3}$ (MPa), where λ is the penetration depth, a is the plasma minor radius, C ($=0.35$) is a constant, $\bar{n}_e$ is the line averaged density, $\bar{T}_e$ is the averaged temperature, and P_0 is the pressure of the

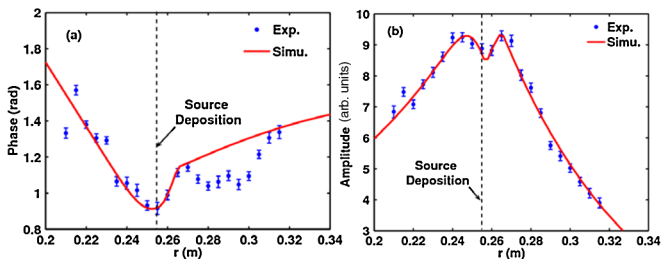

FIG. 4 (color online). Shot no. 7593. Phase (a) and amplitude (b) of the first harmonic of the Fourier transform of the modulated density. Comparison between experiment (circle) and simulation (solid).

beam source. In the present case, $\bar{n}_e \approx 2.5 \times 10^{19}$ m^{-3}, $\bar{T}_e \approx 0.8$ keV, $P_0 \approx 1.3$ MPa; thus, $\lambda \approx 0.144$ m. This value is very close to that determined from the phase minimum: $a - 0.253$ m $= 0.147$ m. From Fig. 4(b), a first peak in amplitude has been found at $r \approx 0.24$ m, slightly shifted inwards compared to the particle source location. This indicates the presence of a significant particle pinch in this region. At the barrier location $r \approx 0.27$ m, a second peak has been found in the amplitude, and strong effect has been observed in the phase.

Now the experimental results have been compared to an analytical model [12] for particle transport to quantitatively characterize this barrier. In cylindrical geometry the particle-transport equation is simply given by

$$\frac{\partial n_e}{\partial t} = \frac{1}{r}\frac{\partial}{\partial r}\left[rD\frac{\partial n_e}{\partial r} + rVn_e\right] + S(r, t),$$

with the following control parameters, the diffusivity D and the convective velocity V. S is the particle source. For the simulation, the following parameters are used: the modulation frequency $f_0 = 9.6$ Hz, the particle deposition $r_{\text{dep}} = 0.253$ m, the minor radius $a = 0.40$ m, the transport barrier is between $x_1 = 0.256$ m and $x_2 = 0.267$ m. In Figs. 4(a) and 4(b), the solid lines represent the simulation. Using the different sensitivities of the phase and amplitude to D and V [13], a satisfactory agreement (best fit) has been found between the experimental points and the analytical calculation, and we have found (Fig. 5) for the particle source described by a Gaussian distribution, the amplitude $S_0 = 0.69 \times 10^{19}$ m^{-1} s^{-1} (the total particle injected per second is $N_p = 2\pi R S_0$), and the width $w = 0.03a$; in domain 1 ($r < x_1$), $D_1 = 0.1$ m^2/s, $V_1 = 1.0$ m/s; in domain 2 or in the well ($x_1 < r < x_2$), $D_2 = 0.045$ m^2/s, $V_2 = -2.7$ m/s; in domain 3 ($r > x_2$), $D_3 = 0.5$ m^2/s, $V_3 = 6.0$ m/s. In the present case the neoclassical Ware pinch [14] $V_{\text{Ware}} \approx \sqrt{r/a}E_\phi/B_\theta \approx 0.6$ m/s around the barrier, where E_ϕ is the toroidal electric field, and B_θ is the poloidal magnetic field. The pinch velocity (positive) found in domain 3 is much larger than the Ware pinch, while the velocity found in domain 1 is very close to the latter. It should be noted that the convective velocity is outward (negative) inside the well. The particle diffusivity found here in the well is very close to the neoclassical value $D_{\text{NC}} \approx 0.03$–$0.04$ m^2/s. For comparison, SMBI modulations have also been performed for a discharge with a density $\bar{n}_e = 1.9 \times 10^{19}$ m^{-3} lower than $\bar{n}_c$. In this case, no barrier has been observed, the diffusivity obtained by this method is $D = 0.25$ m^2/s for $r = 0.28$–0.33 m, and a negative convective velocity has been found $V = -2.2$ m/s for $r = 0.28$–0.31 m, $V = -4.2$ m/s for $r = 0.31$–0.33 m.

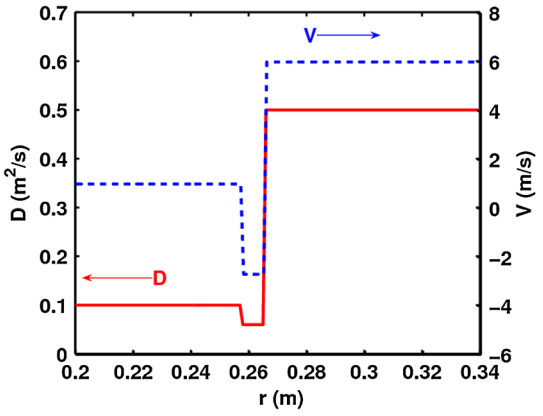

FIG. 5 (color online). Diffusivity D (solid line) and convective velocity V (dashed line) for the simulation of shot no. 7593.

The convective velocity obtained above, using SMBI modulation, can be connected to the turbulent transport models. In tokamaks, an anomalous particle pinch exists in addition to the neoclassical Ware pinch as shown in [15,16]. Theoretical works have shown that this anomalous particle pinch can be driven by turbulence and is composed by two terms: the curvature driven pinch $V_{\nabla q} = -C_q D\nabla q/q$ and the thermodiffusion one $V_{\nabla T} = -C_T D\nabla T_e/T_e$. In the plasma core ($r/a < 0.80$), the electron particle transport is mainly governed by two turbulences: the ion temperature gradient driven modes (ITG) and the electron trapped mode (TEM). As shown in [17,18], for electrons $V_{\nabla q}$ always points inwards, whereas the thermodiffusion term can change direction according to the kind of turbulence: positive or inward for ITG and negative or outward for TEM. As shown in ASDEX-U for Ohmic discharges [19], TEM is dominating for low collisionality (density), while ITG is dominating for high collisionality (density). Calculations with gyrokinetic code GS2 shows that the TEM-ITG transition occurs for an effective collisionality $\nu^*_{\text{eff}} \approx 10$ ($r/a = 0.6$–0.7) [19]. The effective collisionality is defined as $\nu^*_{\text{eff}} = \nu_{ei}/\omega_{De} \approx 10^{-14}$ R $Z_{\text{eff}} n_e T_e^{-2}$, where ν_{ei} is the e-i collision frequency, ω_{De} is the drift frequency, R is the major radius in m, Z_{eff} is the effective ion charge, n_e is the density in m^{-3}, and T_e is the electron temperature in eV. Applying to our case at $r/a = 0.7$, $R = 1.64$ m, $Z_{\text{eff}} \approx 1.5$, $n_e = 1.5 \times 10^{19}$ m^{-3}, $T_e = 0.2$ keV, the effective collisionality corresponding to the threshold $\bar{n}_c$ is $\nu^*_{\text{eff}} \approx 9$, very close to that for TEM-ITG transition. Thus the explanation for the convective velocity found with SMBI modulation could be the following: below the density threshold, TEM is the dominant turbulence, and the convective velocity is negative (outward) since the thermodiffusion dominates. Beyond the threshold, the dominant turbulence is the ITG mode, the convective velocity with thermodiffusion dominance is positive (inward). Inside the transport well, as shown in [20], TEM can be driven by the steep density gradient when a/L_n exceeds a critical value $(a/L_n)_{\text{crit}} \approx 1.6$. In the present case $a/L_n \approx 4$, much larger than the critical value; thus, the corresponding convective velocity is negative inside the transport well. It should be noted that there is an obvious discrepancy between D and V derived from steady profiles and those derived from perturbation

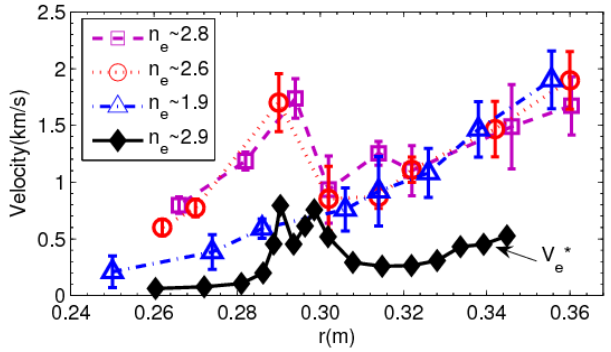

FIG. 6 (color online). Radial profile of the perpendicular turbulence rotation velocity with pITB (○, □) and without pITB (△) measured by Doppler reflectometry. Radial profile of the electron diamagnetic drift velocity V_e^*.

measurements, as that reported in previous works on perturbation transport experiments. The conclusions on the convective velocity are valid only for the perturbed density profile, and not for a stationary density profile.

In order to know if the formation of the pITB is linked or not to the $E_r \times B$ rotation shear and the turbulence reduction, the turbulence perpendicular rotation velocity and its level have been measured with the Doppler reflectometry [21]. The probed turbulence wave number is about $k_s = 5$–$9\ \mathrm{cm}^{-1}$, which is in the wave number range for ITG and TEM. Figures 6 and 7 show, respectively, the radial profile of the turbulence perpendicular rotation velocity and the turbulence level for different densities. Below the critical density $\bar{n}_c = 2.2 \times 10^{19}\ \mathrm{m}^{-3}$, the measured turbulence level and velocity are smoothly increasing with radius for $0.26 < r < 0.36$ m. When density exceeds the threshold, a drastic change in the measured rotation velocity and a significant reduction of the turbulence level have been observed in the barrier region $r = 0.28$–0.30 m. We have also plotted in Fig. 6 the electron diamagnetic drift velocity V_e^*, which is computed from the measured density and

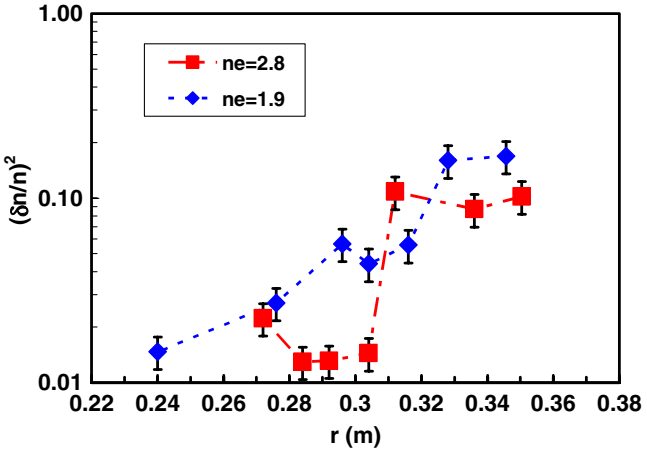

FIG. 7 (color online). Radial profile of the turbulence level with pITB (■) and without pITB (◆) measured by Doppler reflectometry.

electron temperature profiles. The same feature is observed in the barrier region for V_e^*. Assuming $V_\perp = V_{E\times B} + V_e^*$, from Fig. 6, we have roughly $V_{E\times B} \approx 1$ km/s for $0.26 < r < 0.36$ m. This suggests that the drastic change observed in the turbulence rotation velocity at the barrier results from the steepness of the density gradient in the barrier.

In summary pITB phenomena have been experimentally observed in the core region of Ohmic plasmas of the HL-2A tokamak with no externally applied particle or momentum input except the standard gas puffing. A threshold in density has been found for the formation of the pITB with $\bar{n}_c = 2.2 \times 10^{19}\ \mathrm{m}^{-3}$. The diffusivity D is well-like rather than steplike. The convection is inward outside of the well and outward inside the well. For low densities ($\bar{n}_e < \bar{n}_c$) without barrier an outward convective velocity has been found. The change of sign for the convective velocity can be explained by the turbulence TEM-ITG system. During the formation of the barrier, the turbulence level has been reduced inside the barrier region, whereas neither magnetic shear nor $E \times B$ rotation shear underwent great change. On the other hand, the formation of this barrier coincides with the TEM-ITG transition. These suggest that the pITB may be created initially by the discontinuity or jump in the particle diffusivity or the convective velocity during the TEM-ITG transition. These could have interesting implication for the control of the particle-transport barrier via turbulence.

The authors would like to thank Dr. X. Garbet and Dr. G. Giruzzi for fruitful discussions. This work was supported within the framework of the cooperation between the French Commissariat à l'Energie Atomique (CEA) and the China National Nuclear Corporation (CNNC).

[1] F. Wagner *et al.*, Phys. Rev. Lett. **53**, 1453 (1984).
[2] M. J. Greenwald *et al.*, Phys. Rev. Lett. **53**, 352 (1984).
[3] C. L. Fiore *et al.*, Phys. Plasmas **8**, 2023 (2001).
[4] J. E. Rice *et al.*, Nucl. Fusion **42**, 510 (2002).
[5] E. J. Doyle *et al.*, Plasma Phys. Controlled Fusion **42**, A237 (2000).
[6] L. H. Yao *et al.*, Nucl. Fusion **38**, 631 (1998).
[7] N. J. Lopes Cardozo, Plasma Phys. Controlled Fusion **37**, 799 (1995).
[8] P. Mantica *et al.*, Phys. Rev. Lett. **85**, 4534 (2000).
[9] F. Ryter *et al.*, Phys. Rev. Lett. **86**, 2325 (2001).
[10] P. Mantica *et al.*, Phys. Rev. Lett. **96**, 095002 (2006).
[11] L. H. Yao *et al.*, Nucl. Fusion **47**, 1399 (2007).
[12] S. P. Eury *et al.*, Phys. Plasmas **12**, 102511 (2005).
[13] W. W. Xiao *et al.*, Rev. Sci. Instrum. **81**, 013506 (2010).
[14] A. A. Ware, Phys. Rev. Lett. **25**, 916 (1970).
[15] G. T. Hoang *et al.*, Phys. Rev. Lett. **90**, 155002 (2003).
[16] A. Zabolotski, H. Weisen, and TCV Team, Plasma Phys. Controlled Fusion **45**, 735 (2003).
[17] X. Garbet *et al.*, Phys. Rev. Lett. **91**, 035001 (2003).
[18] C. Bourdelle *et al.*, Phys. Plasmas **14**, 112501 (2007).
[19] G. D. Conway *et al.*, Nucl. Fusion **46**, S799 (2006).
[20] D. R. Ernst *et al.*, Phys. Plasmas **11**, 2637 (2004).
[21] W. W. Xiao *et al.*, Plasma Sci. Technol. **10**, 430 (2008).